Mineralogical Magazine, October 2015, Vol. 79(5), pp. 1231–1244

Anzaite-(Ce), a new rare-earth mineral and structure type from the Afrikanda silicocarbonatite, Kola Peninsula, Russia

A.R. Chakhmouradian[1,*], M.A. Cooper[1], L. Medici[2], Y.A. Abdu[1] and Y.S. Shelukhina[3]

[1] Department of Geological Sciences, University of Manitoba, Winnipeg, MB, R3T 2N2 Canada
[2] Istituto di Metodologie per l'Analisi Ambientale, Tito Scalo, 85050 Potenza, Italy
[3] Faculty of Geology, St Petersburg State University, St Petersburg, 199034, Russia

[*Received 17 September 2014; Accepted 15 February 2015; Associate Editor: S.J. Mills*]

ABSTRACT

Anzaite-(Ce), ideally $Ce_4^{3+}Fe^{2+}Ti_6O_{18}(OH)_2$, is a new, structurally complex mineral occurring as scarce minute crystals in hydrothermally altered silicocarbonatites in the Afrikanda alkali-ultramafic complex of the Kola Peninsula, Russia. The mineral is a late hydrothermal phase associated with titanite, hibschite, clinochlore and calcite replacing the primary magmatic paragenesis. The rare-earth elements (*REE*) (dominated by Ce), Ti and Fe incorporated in anzaite-(Ce) were derived from primary Ti oxides abundant in the host rock. Anzaite-(Ce) is brittle and lacks cleavage; the density calculated on the basis of structural data is 5.054(6) g cm^{-3}. The mineral is opaque and grey with a bluish hue in reflected light; its reflectance values range from 15–16% at 440 nm to 13–14% at 700 nm. Its infrared spectrum shows a prominent absorption band at 3475 cm^{-1} indicative of OH^- groups. The average chemical composition of anzaite-(Ce) gives the following empirical formula calculated on the basis of 18 oxygen atoms and two OH^- groups: $(Ce_{2.18}Nd_{0.85}La_{0.41}Pr_{0.26}Sm_{0.08}Ca_{0.36}Th_{0.01})_{\Sigma 4.15}Fe_{0.97}(Ti_{5.68}Nb_{0.22}Si_{0.04})_{\Sigma 5.94}O_{18}(OH)_2$. The mineral is monoclinic, space group $C2/m$, $a = 5.290(2)$, $b = 14.575(6)$, $c = 5.234(2)$ Å, $\beta = 97.233(7)°$, $V = 400.4(5)$ Å^3, $Z = 1$. The ten strongest lines in the X-ray micro-diffraction pattern are [d_{obs} in Å (I) hkl]: 2.596 (100) 002; 1.935 (18) 170; 1.506 (14) 133; 1.286 (13) 1.11.0; 2.046 (12) $\bar{2}41$; 1.730 (12) 003; 1.272 (12) 0.10.2; 3.814 (11) $\bar{1}11$; 2.206 (9) 061; 1.518 (9) 172. The structure of anzaite-(Ce), refined by single-crystal techniques to $R_1 = 2.1\%$, consists of alternating layers of type 1, populated by *REE* (+ minor Ca) in a square antiprismatic coordination and octahedrally coordinated Fe^{2+}, and type 2, built of five-coordinate and octahedral Ti, stacked parallel to (001). This atomic arrangement is complicated by significant disorder affecting the Fe^{2+}, five-coordinate Ti and two of the four anion sites. The order-disorder pattern is such that only one half of these positions in total occupy any given (010) plane, and the disordered (010) planes are separated by ordered domains comprising *REE*, octahedral Ti and two anion sites occupied by O^{2-}. Structural and stoichiometric relations between anzaite-(Ce) and other *REE*-Ti (±Nb, Ta) oxides are discussed. The name anzaite-(Ce) is in honour of Anatoly N. Zaitsev of St Petersburg State University (Russia) and The Natural History Museum (UK), in recognition of his contribution to the study of carbonatites and *REE* minerals. The modifier reflects the prevalence of Ce over other *REE* in the composition of the new mineral.

Keywords: Anzaite-(Ce), new mineral, complex oxide, crystal structure, silicocarbonatite, Afrikanda complex, Kola Peninsula, Russia.

Introduction

In their detailed study of carbonatitic rocks from the Afrikanda complex, Kola Peninsula, Russia (67°25′53″N 32°42′20″E), Chakhmouradian and Zaitsev (1999) noted the presence of an unusual

* E-mail: chakhmou@cc.umanitoba.ca
DOI: 10.1180/minmag.2015.079.5.17

oxide of *REE* and Ti, whose stoichiometry differed appreciably from that of any known *REE*-Ti (±Nb, Ta) oxide. They concluded that the identity of this mineral could be ascertained only with the aid of X-ray diffraction (XRD) techniques, but its further study was delayed by a long search for crystals suitable for XRD analysis. Only recently did careful re-examination of late-stage alteration products of primary platy ilmenite in the Afrikanda silicocarbonatite produce grains of the enigmatic mineral amenable to detailed XRD and spectroscopic examination. The mineral proved to represent a new species and structure type, differing from any known *REE*-Ti oxide not only in the connectivity of cation polyhedra, but also in the presence of significant disorder in the distribution of cations and anions. The new mineral was named anzaite-(Ce) [анзаит-(Ce)] in honour of Anatoly Nikolayevich Zaitsev (b. 1963), Professor of Mineralogy at St Petersburg State University (Russia) and Scientific Associate at the Department of Earth Sciences, The Natural History Museum (London, UK). The name was chosen in recognition of Anatoly Zaitsev's contribution to the study of *REE* minerals, carbonatites and alkaline rocks in the East-African Rift and Kola Peninsula, including Afrikanda (Zaitsev and Chakhmouradian, 2002; Zaitsev *et al.*, 1998, 2004, 2008, 2011; Wall and Zaitsev, 2004, among many others). Both the mineral and its name have been approved by the Commission on New Minerals, Nomenclature and Classification of the International Mineralogical Association (IMA 2013-004, Chakhmouradian *et al.*, 2013). Holotype and cotype specimens (polished sections and unmounted grains) are deposited in the Robert B. Ferguson Museum of Mineralogy at the University of Manitoba (Winnipeg, Canada). All samples come from the same paragenesis and hence were catalogued under the same number, M7888.

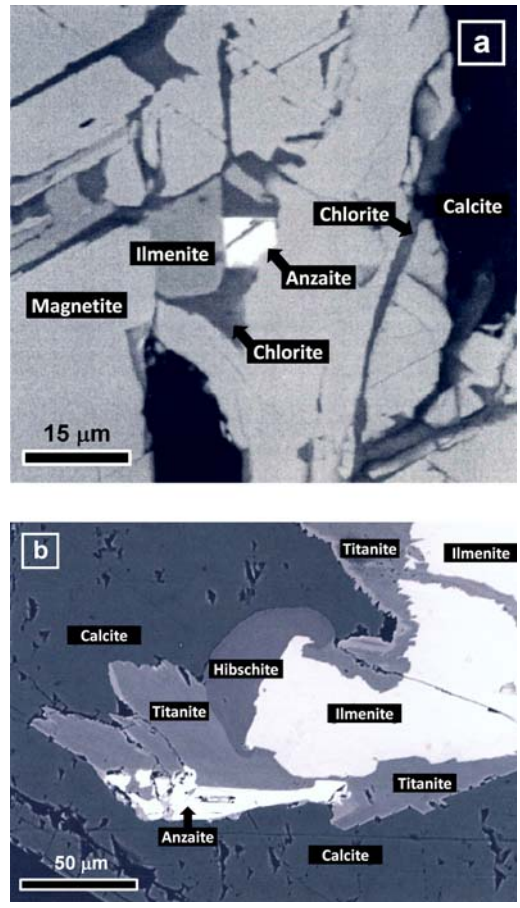

FIG. 1. Textural and paragenetic relations of anzaite-(Ce) with its associated minerals in silicocarbonatite, Afrikanda (Kola Peninsula, Russia); backscattered electron images. (*a*) A subhedral crystal ~8 μm across associated with chlorite developed in fractures in primary ilmenite and Ti-rich magnetite. (*b*) A cluster of subparallel lath-shaped crystals enclosed in titanite mantling primary ilmenite; part of this cluster was studied by infrared and X-ray techniques. Here, hibschite refers to intermediate members of the grossular–katoite solid solution (Chakhmouradian *et al.*, 2008).

Occurrence, paragenesis and crystal morphology

The Afrikanda complex is a multiphase pluton comprising a wide variety of ultramafic, feldspathoid and carbonatitic rocks (Kukharenko *et al.*, 1965). Their emplacement was related to the rifting of the Precambrian Fennoscandian Shield in the Upper Devonian (Kramm *et al.*, 1993; Reguir *et al.*, 2010). In addition to extremely well-preserved igneous assemblages and evidence for differentiation of alkaline undersaturated and carbonatitic magmas (Chakhmouradian and Zaitsev, 2004), the Afrikanda complex hosts hydrothermally reworked clinopyroxenites, pegmatoid ijolites and silicocarbonatites characterized by phenomenally – for such a small locality – diverse mineralogy and compositional variation of individual minerals (Chakhmouradian, 2004; Chakhmouradian and Zaitsev, 1999, 2002; Chakhmouradian *et al.*, 2008; Pekov *et al.*, 1997, 2001; Zaitsev and

TABLE 1. Refectance values (R, %) for anzaite-(Ce).

λ, nm	Average	Range	λ, nm	Average	Range
440	15.3	14.8–15.7	580	13.5	12.8–14.3
460	14.6	13.9–15.1	589	13.6	13.0–14.3
470	14.5	13.8–14.8	600	13.6	13.1–14.3
480	14.3	13.8–14.6	620	13.6	13.3–14.2
500	14.4	13.8–14.7	640	13.7	13.3–14.3
520	14.3	13.4–14.9	650	13.6	13.2–14.2
540	14.0	13.0–14.8	660	13.4	13.0–14.1
546	14.0	13.0–14.8	680	13.5	13.1–13.9
560	13.8	12.9–14.7	700	13.6	13.0–14.2

Chakhmouradian, 2002). For example, 57 minerals have been identified in a ~50 m × 100 m silicocarbonatite body exposed in an open pit in the central part of the complex (Chakhmouradian and Zaitsev, 2004). Apart from anzaite-(Ce), Afrikanda is the type locality for zirconolite (Borodin *et al.*, 1956), cafetite and kassite (Kukharenko *et al.*, 1965; Pekov *et al.*, 2004).

Anzaite-(Ce) is a rare accessory phase in calcite-amphibole-clinopyroxene silicocarbonatite, where this mineral formed at a postmagmatic hydrothermal stage at the expense of primary Ti phases. Its ubiquitous association with ilmenite and/or Ti-rich magnetite (Fig. 1) implies that the latter minerals served as the principal source of Ti and Fe incorporated in anzaite-(Ce). Rare-earth elements were probably derived from perovskite, which is also abundant in the host silicocarbonatite and was affected significantly by postmagmatic processes. Anzaite-(Ce) occurs with titanite, clinochlore, hibschite and late stage calcite (Fig. 1). The fluid regime in which this mineral paragenesis crystallized was estimated as $T \approx 150$–250°C, $a\mathrm{H}^+ \approx 10^{-5}$ and $a\mathrm{H_4SiO_4^o} > 10^{-4}$ (Chakhmouradian and Zaitsev, 2004). Locally observed fracturing of anzaite-(Ce) and its replacement by titanite and the euhedral habit of the former with respect to chlorite (Fig. 1) indicate that the silicate minerals were deposited somewhat later. This is consistent with the overall trend of increasing silica activity in the postmagmatic fluid, manifested in a progressive increase in SiO_2 content in late-stage minerals from the silicocarbonatite (*cf.* tables 4–8 in Chakhmouradian and Zaitsev, 2002).

Anzaite-(Ce) forms sub- to euhedral crystals with an elongate prismatic habit and a diamond-like cross section (possibly, perpendicular to [010]); their length does not exceed 100 μm and width 15 μm (Fig. 1). Some grains are subparallel intergrowths of several crystals, but their mutual orientation could not be ascertained owing to the opacity and weak bireflectance of the mineral.

Physical, optical and spectroscopic characteristics

Macroscopically, anzaite-(Ce) has a greyish black colour and a submetallic lustre. It is opaque, brittle and lacks cleavage. Neither microindentation hardness nor specific gravity of the new mineral could be measured due to the small size of crystals and dearth of material. The calculated density is 5.054(6) g cm^{-3}. In reflected light, the mineral is grey with a slight bluish hue; bireflectance is weak (Table 1). Anzaite-(Ce) does not fluoresce.

A Raman spectrum could not be measured owing to the high susceptibility of anzaite-(Ce) to laser radiation. Even at low power settings, it was ablated easily by a filtered 532 nm laser beam. A Fourier-transform infrared (IR) spectrum was collected on a crystal fragment using a Bruker Hyperion 2000 IR microscope equipped with a liquid nitrogen cooled MCT detector. The spectrum was obtained by averaging 100 scans with a resolution of 4 cm^{-1}. In the O–H stretching region, a prominent sharp absorption band was detected at ~3475 cm^{-1} (Fig. 2), indicating the presence of hydroxyl groups. This was confirmed by structural data (see below).

Chemical composition

The composition of anzaite-(Ce) was determined by wavelength-dispersive X-ray spectrometry (WDS) using an automated CAMECA SX 100 electron

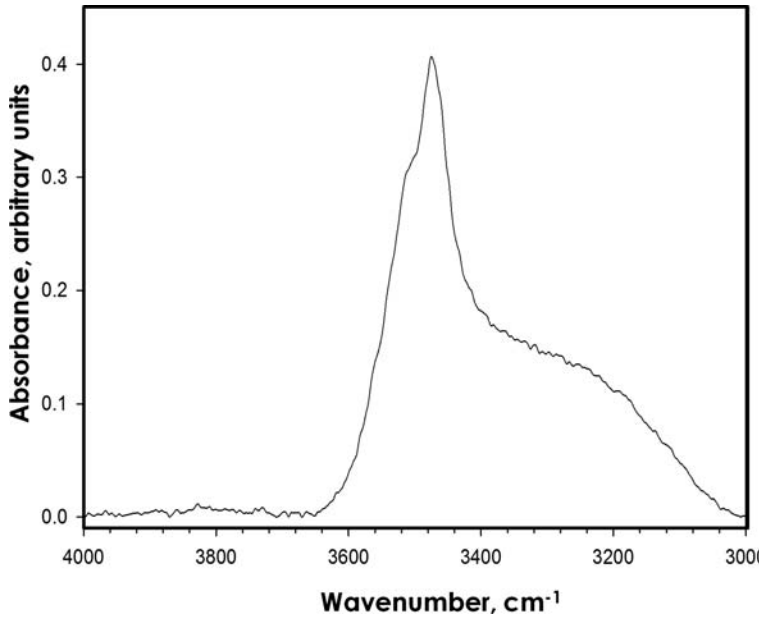

FIG. 2. Fourier transform infrared spectrum of anzaite-(Ce) showing OH stretching vibrations.

microprobe equipped with a backscattered electron (BSE) detector. The instrument was operated at an accelerating voltage of 15 kV, and a beam current of 20 nA; the beam diameter was set at 2 μm. The composition of the new mineral is fairly consistent (Table 2); the low analysis totals (96.5–97.0 wt.%) can be explained by the presence of hydroxyl groups (~1.5 wt.%, according to the structural data) and minor *REE* heavier than Sm. Trace-element analysis by laser ablation techniques was not possible. The average of ten WDS analyses, recalculated on the basis of 18 atoms of oxygen and two OH^- groups (for

TABLE 2. Chemical composition (wt.%) of anzaite-(Ce).

Oxide[a]	Average	Range	Standard deviation	WDS standard
CaO	1.64	1.12–2.48	0.58	Diopside
La_2O_3	5.40	4.85–6.96	0.88	$LaPO_4$ (synthetic)
Ce_2O_3	28.73	26.65–31.52	1.83	$CePO_4$ (synthetic)
Pr_2O_3	3.42	3.04–3.80	0.32	$PrPO_4$ (synthetic)
Nd_2O_3	11.54	9.72–12.44	1.12	$NdPO_4$ (synthetic)
Sm_2O_3	1.18	0.76–1.40	0.25	$SmPO_4$ (synthetic)
ThO_2	0.14	0–0.33	0.13	ThO_2 (synthetic)
FeO	5.63	5.41–5.84	0.17	Fayalite
TiO_2	36.52	35.68–37.44	0.63	Titanite
SiO_2	0.17	0.04–0.28	0.12	Diopside
Nb_2O_5	2.31	0.77–3.47	0.98	$NaBa_2Nb_5O_{15}$ (synthetic)
H_2O (calc.)[b]	1.45			
Total	98.13			

[a] F, Na, Mg, Al, K, Mn, Sr, Zr, Ba, Ta and U were sought, but not detected.
[b] Calculated assuming two OH^- groups in the formula (see Crystal structure).

justification, see below), gives the empirical formula $(Ce_{2.18}Nd_{0.85}La_{0.41}Pr_{0.26}Sm_{0.08}Ca_{0.36}Th_{0.01})_{\Sigma 4.15}Fe_{0.97}(Ti_{5.68}Nb_{0.22}Si_{0.04})_{\Sigma 5.94}O_{18}(OH)_2$, which can be simplified to $Ce_4^{3+}Fe^{2+}Ti_6O_{18}(OH)_2$.

Crystal structure

Refinement

A single-crystal fragment of anzaite-(Ce) measuring 5 μm × 10 μm × 20 μm (Fig. 1*b*) was removed from the polished section after chemical analysis, attached to a tapered glass fibre, and then mounted on a Bruker D8 three-circle diffractometer equipped with a rotating-anode generator (Mo*K*α radiation), multilayer optics and an APEX-II detector. A total of 2348 intensities (the Ewald sphere) was collected to 2θ = 60° using 45 s per 0.2° frame with a crystal-to-detector distance of 50 mm. Empirical absorption corrections (*SADABS*; Sheldrick, 2008) were applied and equivalent reflections were merged, resulting in 616 unique reflections. The unit-cell dimensions were obtained by least-squares refinement of the positions of 2807 reflections with $I > 10\sigma(I)$. The crystal structure of anzaite-(Ce) was solved and refined in space group *C*2/*m* to an R_1 index of 2.1% using the *SHELXL* system of programs (Sheldrick, 2008). Details of the data collection and final structure refinement are provided in Table 3. Atom positions and equivalent displacement parameters are listed in Table 4 and selected interatomic distances and associated bond valences (Brese and O'Keeffe, 1991) are shown in Figs 3 and 4. A list of observed and calculated structure factors and a crystallographic information file have been deposited with the Principal Editor of *Mineralogical Magazine* and are available from www.minersoc.org/pages/e_journals/dep_mat_mm.html.

TABLE 3. Details of single-crystal data collection and crystal-structure refinement for anzaite-(Ce).

Crystal size (μm)	5 × 10 × 20
X-ray wavelength (λ)	0.71073 Å
Temperature (K)	293
Space group	*C*2/*m*
Unit-cell parameters:	
a (Å)	5.290(2)
b (Å)	14.575(6)
c (Å)	5.234(2)
β (°)	97.233(7)
V (Å^3)	400.4(5)
Z	1
Absorption coefficient	14.91 mm^{-1}
F(000)	552
2θ range	5.60–60.28°
Index ranges:	
h	±7
k	±20
l	±7
Reflections:	
Total	7648
Ewald	2348
Unique	616
With $F > 4\sigma(F)$	563
Final agreement factors:	
R_{merge}	3.1%
R_1 [for $F > 4\sigma(F)$]	2.1%
wR_2 (for unique reflections)	5.5%
Goof	1.125
Largest differences	1.47, –1.28

$R_1 = \Sigma(|F_o| - |F_c|) / \Sigma|F_o|$; $wR_2 = [\Sigma w(F_o^2 - F_c^2)^2 / \Sigma w(F_o^2)^2]^{1/2}$; $w = 1 / [\sigma^2(F_o^2) + (0.0327P)^2 + 0.9347P]$, where $P = (\max(F_o^2, 0) + 2F_c^2)/3$.

General comments

Although the structure of anzaite-(Ce) comprises only four cation and four anion sites (Table 4) and is relatively compact ($V \approx 400$ Å^3), its understanding is complicated by significant order-disorder character: one half of the cation and anion sites identified show 50% occupancy and 50% vacancy. In the early stages of refinement, the site occupancies at the partially vacant cation sites were determined to be within the estimated standard deviation (1.5%) of 0.5, and were fixed as such in the final model. Local patterns of atom ordering are readily decipherable using such simple crystal-chemical constraints as atomic distances and bond-valence summations. Below, we present a somewhat expanded description of the structure in an attempt to convey as best we can the architectural complexity of this seemingly simple structure on both local and average scales.

Coordination of the cations

In anzaite-(Ce), the Ti(1) site is coordinated by six O atoms forming a distorted octahedron with a <Ti(1)–O> distance of 1.968 Å (Fig. 3). The refined site-scattering value of 91.2(7) electrons per formula unit (e.p.f.u.) at the Ti(1) site is slightly greater than that expected for full occupancy by Ti (i.e. 88 e.p.f.u.), implying that minor Nb, detected

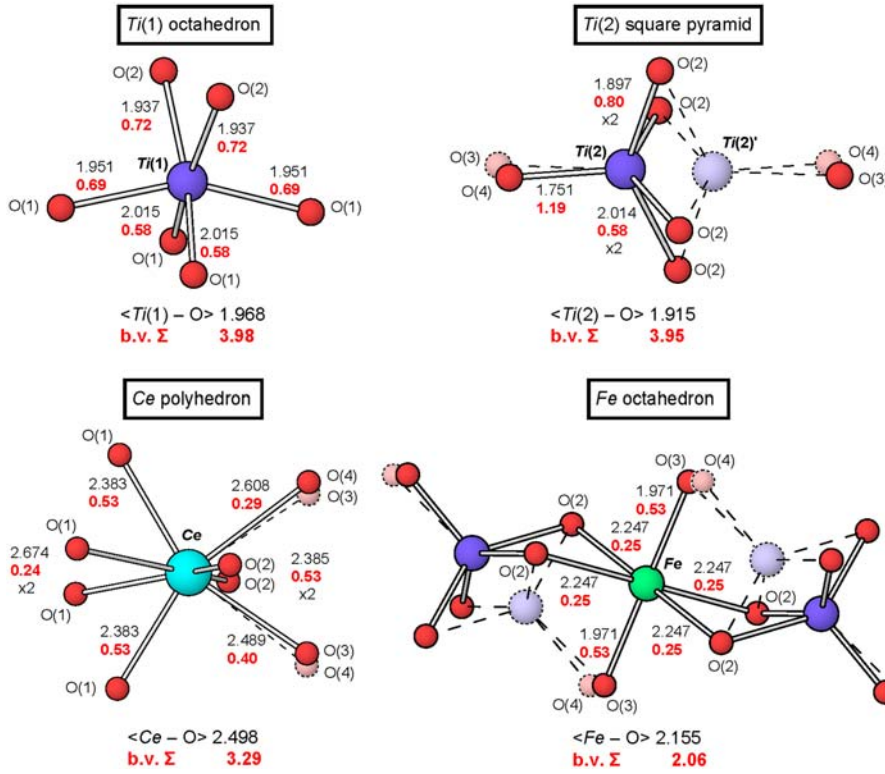

FIG. 3. The cation coordination environments in anzaite-(Ce). Vacant atom positions are indicated by lighter shading, dashed outlines and dashed bonds. Interatomic distances (Å) are given in black lettering, and bond-valence values (vu) in red.

by WDS analysis, is present at Ti(1). The Ti(2) site is positioned just off a two-fold axis and related to the symmetry-equivalent Ti(2)' site located 1.316(4) Å away (Fig. 3). The site occupancy at Ti(2) is, within the estimated standard deviation, 0.5 (see above), i.e. each Ti(2) position is statistically occupied 50% on either side of the two-fold axis, contributing two Ti atoms p.f.u. Unlike Ti(1), the Ti(2) site is coordinated by five anions forming a square pyramid, including four O(2) atoms at the base of the pyramid and one O(4) atom at its apex. Note that the O(3) and O(4) sites are each 50% occupied with a separation of just 0.25(2) Å. When Ti(2) is occupied locally by Ti, the apical O(4) site is occupied by O^{2-} and the adjacent O(3) site is vacant. When Ti(2) is locally vacant, the proximal O(3) site is occupied by $(OH)^{-}$ and the apical O(4) site is vacant. Thus, the O(3)–O(4) anion pair contributes $^{O(3)}(OH)_2 + {}^{O(4)}O_2$ p.f.u. For both Ti coordination spheres, the local anion configurations give very satisfactory bond-valence sums (Fig. 3).

Cerium and other *REE* are located at a single site (Ce), coordinated by seven O^{2-} anions and one $(OH)^{-}$ group [i.e. one O(3) and one O(4) ligand], with an average <Ce–O> distance of 2.498 Å. The refined site occupancy at this site is close to the ideal value, i.e. 234(1) and 232 e.p.f.u., respectively. The Fe site is located at the origin, and is positioned midway between two pairs of disordered Ti(2) sites, with two close Fe–Ti(2) approaches of 2.201(2) Å and two distant approaches of 3.118(2) Å (Fig. 3). The refined site occupancy at the Fe site is 0.5; i.e. when the Fe site is occupied locally by Fe (as in Fig. 3), the two proximal Ti (2) positions on either side are vacant, and the two O(3) sites are occupied by $(OH)^{-}$, resulting in an Fe site octahedrally coordinated by four $^{O(2)}O$ anions and two $^{O(3)}(OH)$ anions. The average <Fe–O> distance of 2.155 Å and a bond-valence sum of 2.06 valence units (vu) indicate unequivocally that this site is occupied by Fe^{2+}. When the Fe site is locally vacant, the two

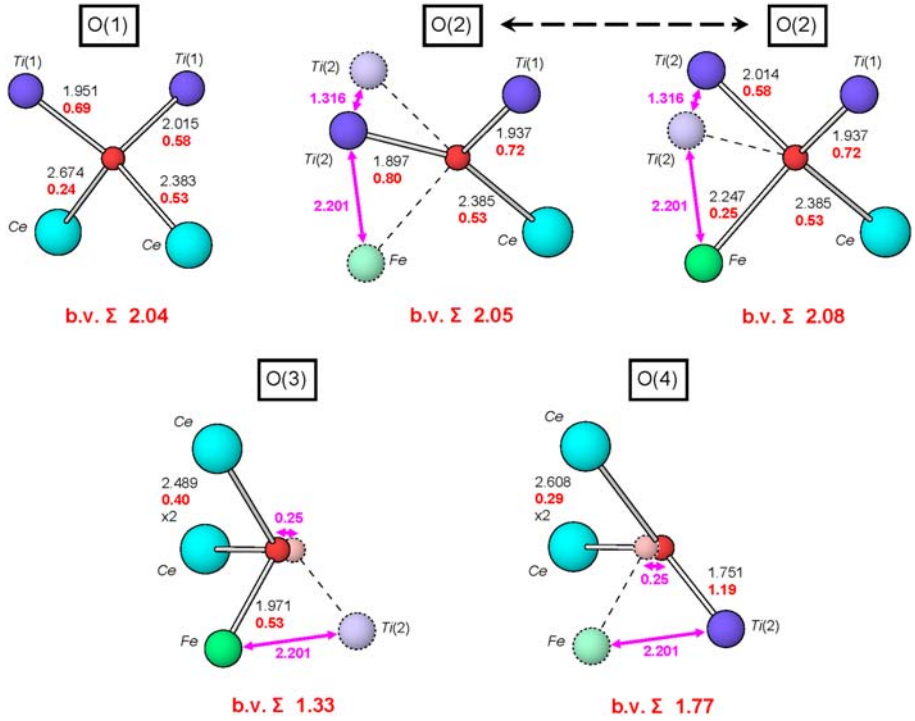

FIG. 4. The anion coordination environments in anzaite-(Ce). Legend as in Fig. 3. Short cation–cation and anion–anion approaches are marked in pink.

proximal Ti(2) positions on either side are occupied by Ti, and the two apical O(4) positions are occupied by O^{2-} anions.

Coordination of the anions

The O(1) site is tetrahedrally coordinated by two Ti(1) and two Ce sites, and the bond-valence sum of 2.04 vu indicates clearly that the O(1) site is occupied by O^{2-} (Fig. 4). Two different coordination environments exist for the O(2) site, one of which is three-coordinate involving Ti(1), Ti(2) and Ce, and the other four-coordinate with Ti(1), Ti(2), Ce and Fe. Note that the Ti(1) and Ce ligands remain constant for each O(2) coordination environment; however, the Ti(2)–ligand distance is longer when the nearby Fe site is occupied and shorter when there is no contribution from Fe^{2+} to O(2). For both O(2) coordination environments, the bond-valence summation at the O(2) anion is ~2 vu, suggesting that the O(2) site is invariably occupied by O^{2-}. The O(3) and O(4) anions are both coordinated by three cations, and their occupancies are coupled to those of the local Ti(2) and Fe sites (Fig. 4). The O(3) anion is coordinated by Ce, Ce and Fe, and the O(4) anion by Ce, Ce and Ti(2). The bond-valence sum at the O(3) anion is 1.33 vu, suggesting that this anion is an OH^- group, and the bond-valence sum at the O(4) anion is 1.77 vu, suggesting that this anion is O^{2-}. Additionally, the O(4) anion acts as a hydrogen bond acceptor, and the bond-valence requirements for both the O(3) and O(4) anions are thus cooperatively satisfied. The donor-acceptor distance is 3.18(1) Å, i.e. the H bond in anzaite-(Ce) is weaker than in hydrated silicate minerals (2.5–3.1 Å: Hammer *et al.*, 1998; Tosoni *et al.*, 2006), but stronger than in some layered hydroxides, such as portlandite (Xu *et al.*, 2007).

Structural connectivity

The crystal structure of anzaite-(Ce) can be described as consisting of alternating layers of Ce–Fe ($z = 0$) and Ti ($z = ½$) polyhedra parallel to (001) (Fig. 5). Note that all of the disordered Ti(2),

TABLE 4. Atom positions and displacement parameters (Å^2) for anzaite-(Ce).

Site	x	y	z	U_{eq}	U^{11}	U^{22}	U^{33}	U^{23}	U^{13}	U^{12}
Ce	0	0.35833(2)	0	0.01139(12)	0.00901(16)	0.01668(19)	0.00856(17)	0	0.00137(10)	0
Ti(1)	0	0.19539(7)	½	0.0085(3)	0.0058(5)	0.0104(5)	0.0095(5)	0	0.0015(3)	0
Ti(2)	0.5885(4)	½	0.4223(4)	0.0103(5)	0.0102(9)	0.0093(10)	0.0119(10)	0	0.0028(8)	0
Fe	½	½	0	0.0159(6)	0.0117(11)	0.0186(13)	0.0175(13)	0	0.0021(9)	0
O(1)	0.2542(6)	0.2250(2)	0.2733(6)	0.0106(7)	0.0110(14)	0.0137(15)	0.0079(13)	–0.0020(11)	0.0043(11)	–0.0024(12)
O(2)	0.3577(6)	0.5934(2)	0.2923(6)	0.0145(7)	0.0170(14)	0.0111(15)	0.0137(14)	–0.0011(12)	–0.0051(11)	0.0030(12)
O(3)	0.844(3)	½	0.195(2)	0.0152(14)*						
O(4)	0.847(3)	½	0.243(2)	0.0152(14)*						

*Constrained to be equal during refinement.

Fe, O(3) and O(4) sites are shown spread along the (010) plane at $y = 0$, ½, but only half of these positions in total occupy any given (010) plane. These (010) planes of disordered Ti(2)–Fe–O(3)–O(4) are separated by ordered Ce–Ti(1)–O(1)–O(2) regions. The connectivity of the Ti polyhedra [(001) layer, $z = ½$] is shown in Fig. 6, with crankshaft edge-sharing Ti(1) octahedral chains running parallel to [100], connected by edge-sharing Ti(2) square pyramids. On the left hand side of Fig. 6, the Ti(2)–Ti(2)' pairings are shown in ball and stick representation (with an imposed local ordering). The remaining Ti(2) sites are shown in polyhedral representation, with an arbitrary Ti(2) ordering scheme for a given (010) plane. The Ti layer in anzaite-(Ce) can be described as an edge-sharing polyhedral sheet composed of Ti octahedra and Ti square pyramids in a 2 to 1 ratio and containing eight-membered polyhedral rings of the form $^{[6]}Ti_6{}^{[5]}Ti_2$. The connectivity of the eight-coordinate Ce sites and Fe^{2+} octahedra [(001) layer, $z = 0$] is shown in Fig. 7. The Ce polyhedra share edges along [100] and [010], forming six-membered rings that contain either an Fe octahedron or a vacancy at the centre of the ring. On the left side of Fig. 7, an imposed local ordering of Fe sites along [100] is shown in ball and stick representation, and the remainder of the Fe sites are shown in polyhedral representation, with an arbitrary Fe ordering scheme for a given (010) plane. A disordered (010) plane is shown in plan view in Fig. 8. The Ti(2), Fe, O(3) and O(4) sites are shown with an imposed local ordering that propagates laterally in all directions, i.e. when one begins with a given single Fe site occupied by Fe^{2+}, all remaining Ti(2) + Fe + O(3) + O(4) sites within a given (010) plane become configured as either occupied or vacant (Fig. 8*a*). To aid in visualization, this ordered arrangement is replicated in polyhedral representation in Fig. 8*b*. The Fe octahedra share four edges with four Ce polyhedra in the (001) plane (Fig. 7), and additionally share two opposing edges with two Ti(2) square pyramids in the (010) plane (Fig. 8*b*). Also shown is the resulting ordered hydrogen-bonding scheme [O(3)–H···O(4)]. The structure of anzaite-(Ce) can therefore be thought of as locally ordered individual (010) layers (like that in Fig. 8), in which the individual ordering scheme in a given (010) layer does not couple to that in the next (010) layer. The two possible ordering schemes of the (010) layer occur with equal probability, resulting in the 50% occupancy of the Ti(2), Fe, O(3) and O(4) sites.

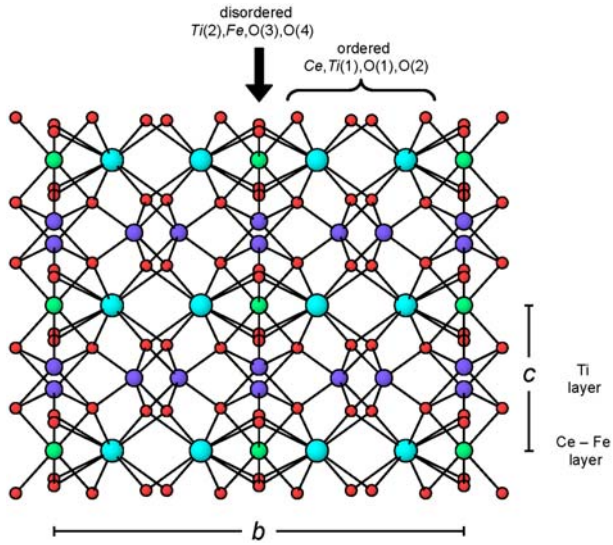

FIG. 5. The crystal structure of anzaite-(Ce) shown projected onto (100). Alternating Ce–$Fe_{(z=0)}$ and $Ti_{(z=½)}$ layers parallel to (001), and ordered/disordered (010) regions of the structure are labelled.

X-ray micro-diffraction

An X-ray micro-diffraction (μ-XRD) pattern of anzaite-(Ce) was collected *in situ* from a polished section using a Rigaku D/max-RAPID diffractometer operated at 40 kV and 30 mA. This instrument is equipped with a curved-image-plate detector, flat graphite monochromator, variety of beam collimators, motorized stage and microscope for accurate positioning of the sample. The stage allows two angular movements (rotation ϕ and revolution ω). The data were collected in reflection mode using various sample-to-beam geometries and operating conditions. Using a 30 μm collimator and collection times ranging from 12 to 18 hours, several datasets were obtained with ω fixed and ϕ ranging from 0° (four data subsets at different positions) to 20° (one subset), 25° (two subsets), 50° and 70° (one subset each). The results obtained with these different acquisition parameters are mutually consistent. The XRD data were collected as two-dimensional images and then converted into 2*d*–*I* profiles using Rigaku R-Axis Display software. The integrated XRD pattern (Table 5) was indexed on a monoclinic

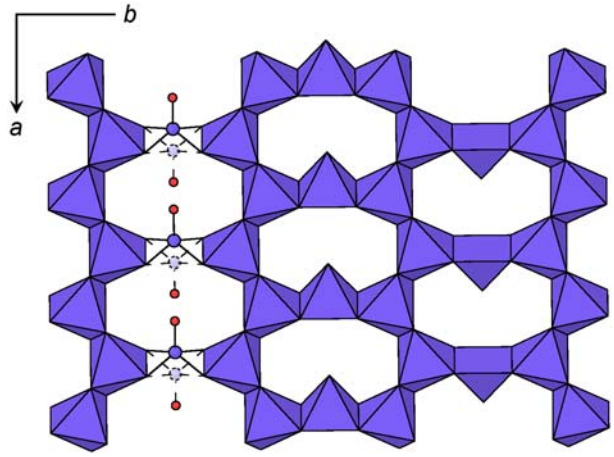

FIG. 6. The Ti layer of the anzaite-(Ce) crystal structure projected down [001] at $z = ½$.

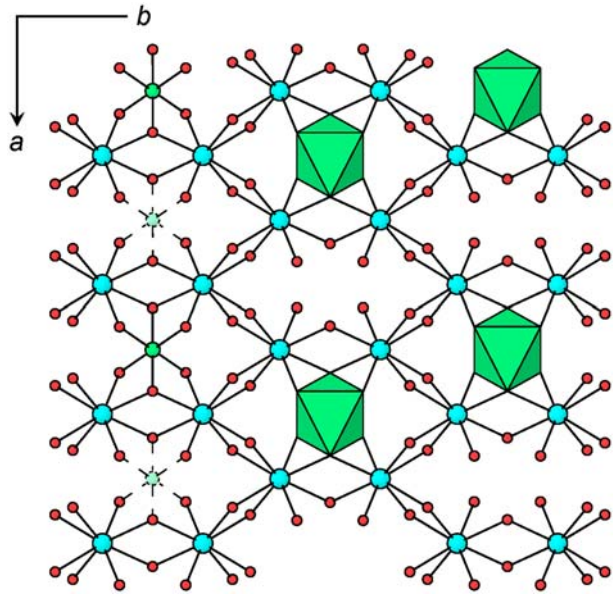

FIG. 7. The Ce–Fe layer of the anzaite-(Ce) crystal structure projected down [001] at $z = 0$.

C/2*m* cell determined from the single-crystal data. The cell parameters, refined using the *UnitCell* software of Holland and Redfern (1997), are consistent with the results of single-crystal refinement: $a = 5.293(1)$, $b = 14.586(3)$, $c = 5.233(1)$ Å, $\beta = 97.30(2)°$, $V = 400.7(2)$ Å^3.

Classification and distinction from other mineral species

Anzaite-(Ce) is a multiple oxide (Dana Class 04) representing a new structure type clearly distinct from any other naturally occurring *REE*-Ti oxide. Because

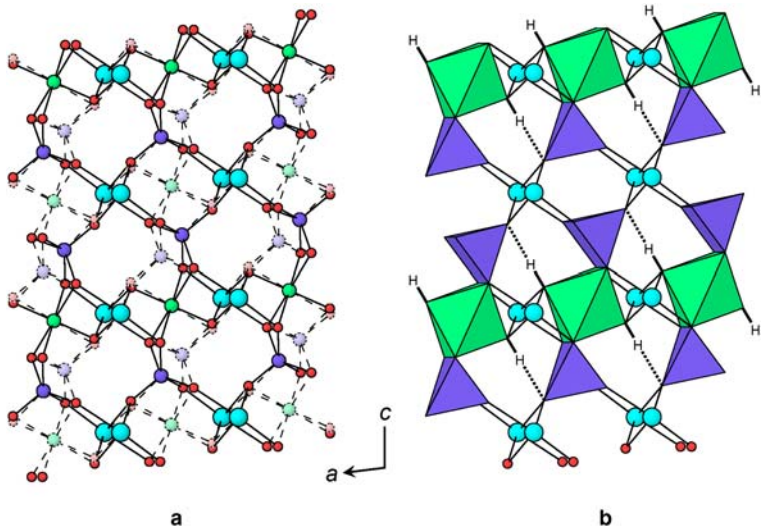

FIG. 8. Local ordering of Ti(2)–Fe–O(3)–O(4) within a given (010) plane ($y = 0$; ½) of the anzaite-(Ce) crystal structure, projected down an axis 10° from [010]; (*a*) ball and stick representation; (*b*) polyhedral representation with additional H-bonding shown. Legend as in Fig. 3.

TABLE 5. Micro-XRD data for anzaite-(Ce).

I	h	k	l	d_{meas}	d_{calc}
1	1	1	0	4.941	4.940
11	**$\bar{1}$**	**1**	**1**	**3.814**	**3.813**
4	**$\bar{1}$**	3	1	3.07	3.066
3	0	4	1	2.986	2.984
1	1	3	1	2.828	2.828
2	2	0	0	2.628	2.625
100	**0**	**0**	**2**	**2.596**	**2.595**
3	1	5	0	2.553	2.550
1	$\bar{2}$	0	1	2.472	2.473
1	2	2	0	2.469	2.470
1	0	2	2	2.443	2.445
1	0	6	0	2.429	2.431
1	$\bar{1}$	1	2	2.418	2.420
1	$\bar{2}$	2	1	2.338	2.342
1	1	5	1	2.233	2.235
4	2	0	1	2.228	2.231
9	**0**	**6**	**1**	**2.206**	**2.202**
3	1	1	2	2.194	2.192
1	0	4	2	2.114	2.114
12	**$\bar{2}$**	**4**	**1**	**2.046**	**2.047**
2	1	3	2	2.021	2.017
3	**$\bar{2}$**	0	2	1.974	1.975
18	**1**	**7**	**0**	**1.935**	**1.937**
4	**$\bar{2}$**	2	2	1.908	1.907
4	2	4	1	1.903	1.903
4	$\bar{1}$	5	2	1.878	1.878
1	$\bar{1}$	7	1	1.841	1.843
1	2	6	0	1.782	1.784
1	0	6	2	1.775	1.774
1	1	5	2	1.765	1.765
6	3	1	0	1.738	1.738
4	$\bar{2}$	6	1	1.734	1.734
12	**0**	**0**	**3**	**1.730**	**1.730**
6	0	8	1	1.718	1.720
6	$\bar{3}$	1	1	1.714	1.714
6	$\bar{1}$	1	3	1.696	1.697
1	0	2	3	1.682	1.683
2	3	3	0	1.648	1.647
3	2	6	1	1.644	1.644
1	3	1	1	1.59	1.589
1	1	1	3	1.575	1.575
3	0	4	3	1.563	1.563
4	1	9	0	1.549	1.549
2	$\bar{2}$	6	2	1.533	1.533
9	**1**	**7**	**2**	**1.518**	**1.518**
14	**1**	**3**	**3**	**1.506**	**1.506**
7	0	8	2	1.492	1.492
2	$\bar{3}$	5	1	1.487	1.486
1	0	10	0	1.457	1.459
1	$\bar{2}$	4	3	1.418	1.416
2	2	6	2	1.415	1.414
2	2	8	1	1.411	1.412
2	0	10	1	1.404	1.404
2	3	5	1	1.400	1.402
1	1	5	3	1.393	1.392
1	2	0	3	1.367	1.367
1	3	1	2	1.366	1.366
2	$\bar{1}$	9	2	1.351	1.352
3	2	2	3	1.343	1.344
5	$\bar{2}$	8	2	1.340	1.340
1	$\bar{3}$	7	1	1.330	1.329
2	3	3	2	1.320	1.321
2	4	0	0	1.313	1.313
2	1	9	2	1.308	1.308
6	$\bar{2}$	6	3	1.300	1.299
13	**1**	**11**	**0**	**1.286**	**1.286**
2	2	4	3	1.279	1.280
12	**0**	**10**	**2**	**1.272**	**1.272**
4	3	7	1	1.267	1.268
2	1	7	3	1.262	1.261
2	2	8	2	1.258	1.258
2	$\bar{1}$	3	4	1.254	1.255
1	1	11	1	1.240	1.239
3	4	0	1	1.236	1.236
2	$\bar{2}$	0	4	1.227	1.227
2	2	10	1	1.221	1.221
2	1	1	4	1.219	1.220
1	0	12	0	1.215	1.216
3	$\bar{2}$	2	4	1.209	1.210
1	3	9	0	1.190	1.189
4	1	3	4	1.187	1.187
4	0	12	1	1.184	1.184
4	$\bar{3}$	9	1	1.181	1.182
1	$\bar{1}$	9	3	1.176	1.176
1	$\bar{2}$	8	3	1.175	1.175
1	$\bar{2}$	10	2	1.174	1.173
2	4	4	1	1.171	1.170
2	$\bar{1}$	11	2	1.167	1.167
1	$\bar{2}$	4	4	1.163	1.163
2	3	3	3	1.127	1.127
4	$\bar{3}$	9	2	1.119	1.118

(continued)

TABLE 5. (*contd*.)

The ten strongest lines are given in bold.

of its structural uniqueness, anzaite-(Ce) cannot be assigned to any of the existing mineral groups among multiple *REE*-Ti oxides. The latter most typically show stoichiometry of the type AB_2X_6, where A = *REE* (±Ca, Th, U); B = Ti, Nb, Ta (±Fe); X = O or OH and, hence, an A/B ratio of 0.5, i.e. appreciably lower than in anzaite-(Ce). The most common minerals of this type are members of the aeschynite and euxenite groups that crystallize with orthorhombic symmetry (*Pnma* and *Pbcn*, respectively: Thorogood *et al.*, 2010) and differ significantly

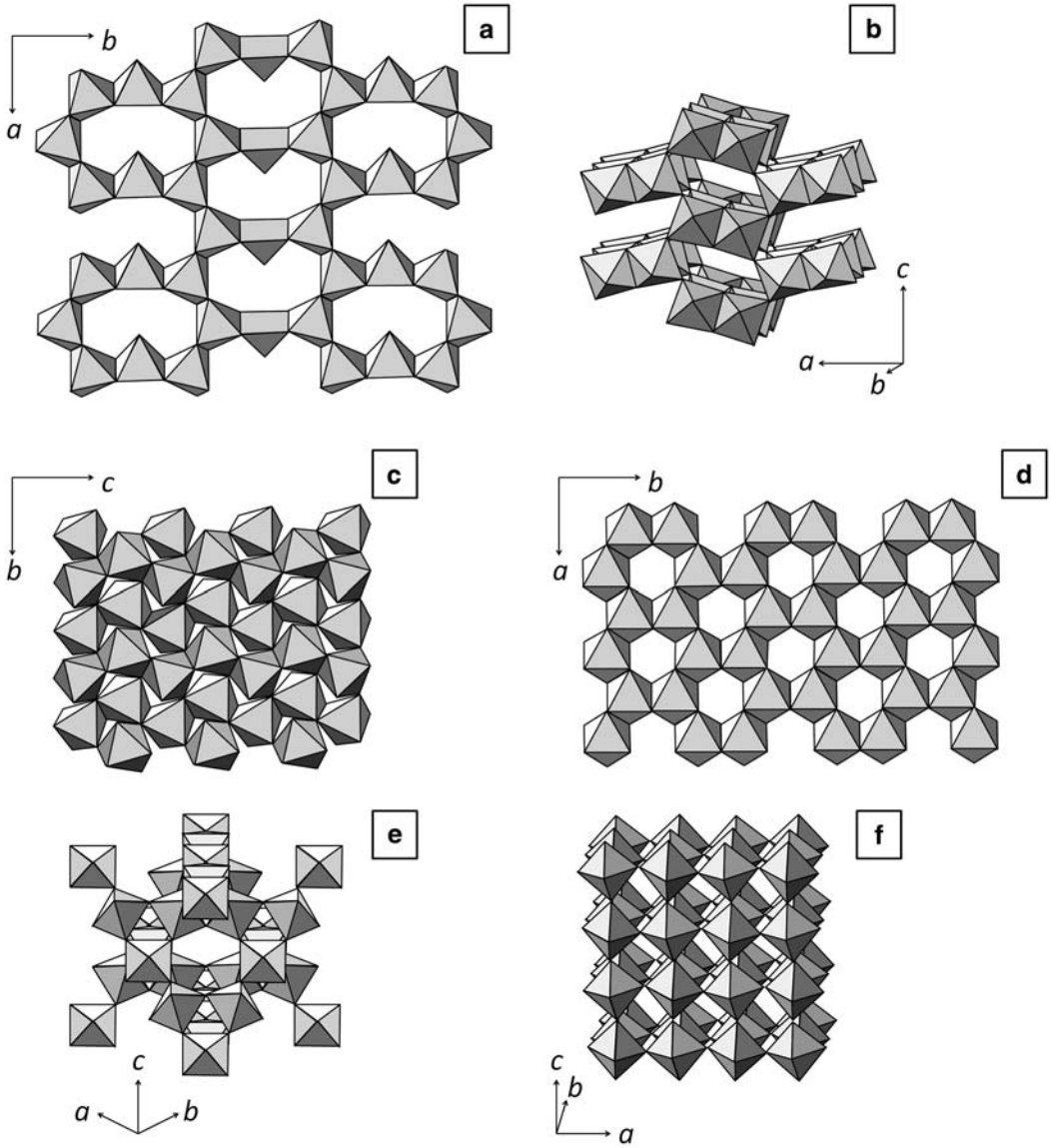

FIG. 9. Schematic diagram showing the connectivity of Ti (±Nb, Ta) polyhedra in the structure of anzaite-(Ce) and other *REE*-Ti oxides. (*a*) Layer of Ti-centred polyhedra in anzaite-(Ce); *REE* in square-antiprismatic coordination and Fe^{2+}-centred octahedra are sandwiched between these layers (see Figs 3–8 for details). (*b*) Framework of edge- and corner-sharing $(Ti,Nb,Ta)O_6$ in aeschynite; *REE* in a bicapped, trigonal prismatic coordination are accommodated within tunnels in the framework. (*c*) Double-decked layer of $(Ti,Nb,Ta)O_6$ in euxenite; *REE* in a square antiprismatic configuration are sandwiched between these layers (Thorogood *et al.* 2010). (*d*) Layer of Ti-centred octahedra in lucasite-(Ce); *REE* in a distorted square-antiprismatic coordination are sandwiched between these layers (Nickel *et al.*, 1987). (*e*) Open framework of corner-sharing TiO_6 octahedra in pyrochlores $(Sm–Lu)_2Ti_2O_7$ with voids accommodating *REE* in a cubic coordination (Helean *et al.*, 2004); the latter sites are commonly vacant in natural pyrochlores (e.g. ~60% vacancies in ceriobetafite; Mitchell and Chakhmouradian, 1998). (*f*) Compact framework of corner-sharing TiO_6 octahedra in the cation-deficient orthorhombic perovskite $La_{0.6}Ca_{0.1}TiO_3$ (Zheng *et al.*, 2007); cubo-octahedrally coordinated La and Ca occupy voids in this scaffolding.

from anzaite-(Ce) in structural topology (Fig. 9). Lucasite-(Ce), *REE*Ti_2O_5OH, is also a monoclinic layered titanate, but differs from anzaite-(Ce) structurally (*I*/2*a*, $a = 5.18$, $b = 8.76$, $c = 9.77$ Å, $\beta = 93.5°$, $Z = 4$: Nickel *et al.*, 1987). If single crystals are unavailable, the two minerals can be readily distinguished on the basis of their cation ratios and powder XRD patterns. The intense lines at 4.45, 3.26 and 3.20 Å in lucasite-(Ce) are not observed in anzaite-(Ce) (Table 5). Pyrochlore-type phases, whose stoichiometry is extremely variable ($A_{2-x}B_2X_{7-y}$), may approach anzaite-(Ce) in composition if $A = REE$, $B = Ti$, $x = 0.8–0.9$ and $y = 1.2–1.3$ (e.g. Chtoun *et al.*, 2001). However, pyrochlores are isometric (space group $Fd3m$, $a \approx 10.2$ Å) and have a completely different atomic arrangement comprising an open framework of BX_6 octahedra (Fig. 9). According to experimental data, both pyrochlore and euxenite structures favour *REE* heavier than Nd (Helean *et al.*, 2004; Thorogood *et al.*, 2010), whereas anzaite-(Ce) and lucasite-(Ce) are dominated by light lanthanides, and naturally occurring aeschynite can be either light or heavy *REE* dominant (Bonazzi and Menchetti, 1999). Finally, perovskite-type phases (ideally, ABX_3) can develop significant cation deficiency in the *A* site. The only natural example known to date is a hydrothermally altered derivative of loparite-(Ce), referred to as 'metaloparite' in the literature. This mineral has ~50% deficiency (x) of cations (mostly light *REE*) in the *A* site and is hydrated and metamict, but regains partial crystallinity upon heating to $T \geq 750$°C (Chakhmouradian *et al.*, 1999). A plethora of perovskite-type titanates has been synthesized with light lanthanides and a variety of other large cations substituting in the *A* site, and x ranging from nil to 33% (Ruiz *et al.*, 2002; Zhang *et al.*, 2007). These compounds are low-symmetry derivatives of the isometric archetype ($Pm3m$, $a \approx 3.9$ Å) but retain the same structural motif comprising corner sharing BX_6 octahedra (Fig. 9). It is very likely that, in the future, cation-deficient perovskites similar to these synthetic compounds will be recognized in Nature. Given their potentially variable stoichiometry, an XRD study will be required to confirm their identity and distinguish them from anzaite-(Ce).

Acknowledgements

This work was supported by the Natural Sciences and Engineering Research Council of Canada. The authors are grateful to Frank C. Hawthorne (University of Manitoba), for access to the X-ray facilities at the University of Manitoba. The present manuscript benefitted greatly from reviews by Ray Macdonald, Ritsuro Miyawaki and Peter Leverett.

References

Bonazzi, P. and Menchetti, S. (1999) Crystal chemistry of aeschynite-(Y) from the Western Alps: residual electron density on difference-Fourier map. *European Journal of Mineralogy*, **11**, 1043–1049.

Borodin, L.S., Nazarenko, I.I. and Rikhter, T.L. (1956) On the new mineral zirconolite, a complex oxide of AB_3O_7 type. *Doklady Akademii Nauk SSSR*, **110**, 845–848.

Brese, N.E. and O'Keeffe, M. (1991) Bond-valence parameters for solids. *Acta Crystallographica*, **B47**, 192–197.

Chakhmouradian, A.R. (2004) Crystal chemistry and paragenesis of compositionally unique (Al-, Fe-, Nb- and Zr-rich) titanite from Afrikanda, Russia. *American Mineralogist*, **89**, 1752–1762.

Chakhmouradian, A.R. and Zaitsev, A.N. (1999) Calcite-amphibole-clinopyroxene rock from the Afrikanda complex, Kola Peninsula (Russia): mineralogy and a possible link to carbonatites. Part I: Oxide minerals. *The Canadian Mineralogist*, **37**, 177–198.

Chakhmouradian, A.R. and Zaitsev, A.N. (2002) Calcite-amphibole-clinopyroxene rock from the Afrikanda complex, Kola Peninsula, Russia: mineralogy and a possible link to carbonatites. III. Silicate minerals. *The Canadian Mineralogist*, **40**, 1347–1374.

Chakhmouradian, A.R. and Zaitsev, A.N. (2004) Afrikanda: an association of ultramafic, alkaline and alkali-silica-rich carbonatitic rocks from mantle-derived melts. Pp. 247–291 in: *Phoscorites and Carbonatites from Mantle to Mine: The Key Example of the Kola Alkaline Province* (F. Wall and A.N. Zaitsev, editors). Mineralogical Society of Great Britain and Ireland, London.

Chakhmouradian, A.R., Mitchell, R.H., Pankov, A.V. and Chukanov, N.V. (1999) Loparite and 'metaloparite' from the Burpala alkaline complex, Baikal Alkaline Province (Russia). *Mineralogical Magazine*, **63**, 519–534.

Chakhmouradian, A.R., Cooper, M.A., Medici, L., Hawthorne, F. and Adar, F. (2008) Fluorine-rich hibschite from silicocarbonatite, Afrikanda complex, Russia: crystal chemistry and conditions of crystallization. *The Canadian Mineralogist*, **46**, 1033–1042.

Chakhmouradian, A.R., Cooper, M.A., Medici, L., Abdu, Y.A. and Shelukhina, Y.S. (2013) Anzaite-(Ce), IMA 2013-004. CNMNC Newsletter No. 16, August 2013, page 2701; *Mineralogical Magazine*, **77**, 2695–2709.

Chtoun, E.H., Hanebali, L. and Garnier, P. (2001) Analyse par diffraction des rayons X, methode de Rietveld, de la structure des solutions solides $(1–x)A_2Ti_2O_7 – xFe_2TiO_5$ A = Eu, Y. *Annales de Chimie Science des Matériaux*, **26**, 27–32.

Hammer, V.M.F., Libowitzky, E. and Rossman, G.R. (1998) Single-crystal IR spectroscopy of very strong hydrogen bonds in pectolite, $NaCa_2[Si_3O_8(OH)]$, and serandite, $NaMn_2[Si_3O_8(OH)]$. *American Mineralogist*, **83**, 569–576.

Helean, K.B., Ushakov, S.V., Brown, C.E., Navrotsky, A., Lian, J., Ewing, R.C., Farmer, J.M. and Boatner, L.A. (2004) Formation enthalpies of rare earth titanate pyrochlores. *Journal of Solid State Chemistry*, **177**, 1858–1866.

Holland, T.J.B. and Redfern, S.A.T. (1997) Unit cell refinement from powder diffraction data: the use of regression diagnostics. *Mineralogical Magazine*, **61**, 65–77.

Kramm, U., Kogarko, L.N., Kononova, V.A. and Vartiainen, H. (1993) The Kola Alkaline Province of the CIS and Finland: precise Rb-Sr ages define 380–360 Ma age range for all magmatism. *Lithos*, **30**, 33–44.

Kukharenko, A.A., Orlova, M.P., Bulakh, A.G., Bagdasarov, E.A., Rimskaya-Korsakova, O.M., Nefedov, Y.I., Ilyinskiy, G.A., Sergeyev, A.C. and Abakumova, N.B. (1965) *The Caledonian Complex of Ultrabasic Alkaline Rocks and Carbonatites of the Kola Peninsula and Northern Karelia.* Nedra Press, Moscow.

Mitchell, R.H. and Chakhmouradian, A.R. (1998) Th-rich loparite from the Khibina alkaline complex, Kola Peninsula: isomorphism and paragenesis. *Mineralogical Magazine*, **62**, 341–353.

Nickel, E.H., Grey, I.E. and Madsen, I.C. (1987) Lucasite-(Ce), $CeTi_2(O,OH)_6$, a new mineral from Western Australia: Its description and crystal structure. *American Mineralogist*, **72**, 1006–1010.

Pekov, I.V., Petersen, O.V. and Voloshin, A.V. (1997) Calcio-ancylite-(Ce) from Ilímaussaq and Narssârssuk, Greenland, Kola Peninsula and Polar Urals, Russia; ancylite-(Ce) – calcio-ancylite-(Ce) an isomorphous series. *Neues Jahrbuch für Mineralogie, Abhandlungen*, **171**, 309–322.

Pekov, I.V., Turchkova, A.G. and Kulikova, I.M. (2001) Barium and potassium zeolites from the Afrikanda alkaline massif (Kola Peninsula). *Proceedings of the Workshop on Alkaline Magmatism*, Moscow, pp. 56–57.

Pekov, I.V., Schneider, J. and Pushcharovsky, D.Y. (2004) On the X-ray powder diffractogram of kassite and its relationship with cafetite. *Zapiski Vserossiiskogo Mineralogicheskogo Obshchestva*, **133(3)**, 51–54.

Reguir, E.P., Camacho, A., Yang, P., Chakhmouradian, A. R., Kamenetsky, V.S. and Halden, N.M. (2010) Trace-element study and uranium-lead dating of perovskite from the Afrikanda plutonic complex, Kola Peninsula (Russia) using LA-ICP-MS. *Mineralogy and Petrology*, **100**, 95–103.

Ruiz, A.I., López, M.L., Pico, C. and Veiga, M.L. (2002) New $La_{2/3}TiO_3$ derivatives: structure and impedance spectroscopy. *Journal of Solid State Chemistry*, **163**, 472–478.

Sheldrick, G.M. (2008) A short history of SHELX. *Acta Crystallographica*, **A64**, 112–122.

Thorogood, G.J., Avdeev, M. and Kennedy, B.J. (2010) Structural studies of the aeschynite-euxenite transformation in the series $Ln(TiTa)O_6$ *Ln* = Lanthanide. *Solid State Sciences*, **12**, 1263–1269.

Tosoni, S., Doll, K. and Ugliengo, P. (2006) Hydrogen bond in layered materials: structural and vibrational properties of kaolinite by a periodic B3LYP approach. *Chemistry of Materials*, **18**, 2135–2143.

Wall, F. and Zaitsev, A.N. (2004) Rare earth minerals in Kola carbonatites. Pp. 43–72 in: *Phoscorites and Carbonatites from Mantle to Mine: The Key Example of the Kola Alkaline Province* (F. Wall and A.N. Zaitsev, editors). Mineralogical Society of Great Britain and Ireland, London.

Xu, H., Zhao, Y., Vogel, S.C., Daemen, L.L. and Hickmott, D.D. (2007) Anisotropic thermal expansion and hydrogen bonding behaviour of portlandite: a high-temperature neutron diffraction study. *Journal of Solid State Chemistry*, **180**, 1519–1525.

Zaitsev, A.N. and Chakhmouradian, A.R. (2002) Calcite-amphibole-clinopyroxene rock from the Afrikanda complex, Kola Peninsula, Russia: mineralogy and a possible link to carbonatites. II. Oxysalt minerals. *The Canadian Mineralogist*, **40**, 103–120.

Zaitsev, A.N., Wall, F. and Le Bas, M.J. (1998) REE-Sr-Ba minerals from the Khibina carbonatites, Kola Peninsula, Russia: their mineralogy, paragenesis and evolution. *Mineralogical Magazine*, **62**, 225–250.

Zaitsev, A.N., Keller, J., Spratt, J., Perova, E.N. and Kearsley, A. (2008) Nyerereite – pirssonite – calcite – shortite relationships in altered natrocarbonatites, Oldoinyo Lengai, Tanzania. *The Canadian Mineralogist*, **46**, 843–860.

Zaitsev, A.N., Sitnikova, M.A., Subbotin, V.V., Fernández-Suárez, J. and Jeffries, T.E. (2004) Sallanlatvi Complex – a rare example of magnesite and siderite carbonatites. Pp. 201–245 in: *Phoscorites and Carbonatites from Mantle to Mine: The Key Example of the Kola Alkaline Province* (F. Wall and A. N. Zaitsev, editors). Mineralogical Society of Great Britain and Northern Ireland, London.

Zaitsev, A.N., Chakhmouradian, A.R., Siidra, O.I., Spratt, J., Williams, C.T., Stanley, C.J., Petrov, S.V., Britvin, S.N. and Polyakova, E.A. (2011) Fluorine-, yttrium- and lanthanide-rich cerianite from carbonatitic rocks of the Kerimasi volcano and surrounding explosion craters, Gregory Rift, northern Tanzania. *Mineralogical Magazine*, **75**, 2801–2810.

Zheng, Z., Lumpkin, G.R., Howard, C.J., Knight, K.S., Whittle, K.R. and Osaka, K. (2007) Structures and phase diagrams for the system $CaTiO_3$–$La_2/_3TiO_3$. *Solid State Chemistry*, **180**, 1083–1092.